European Polymer Journal 102 (2018) 68–74

Contents lists available at ScienceDirect

European Polymer Journal

journal homepage: www.elsevier.com/locate/europolj

Thermal transitions in hyperbranched polyester-polyol assemblies on carbon

E.D. Farias[a], M.C.G. Passeggi Jr.[a,b], V. Brunetti[c,*]

[a] Laboratorio de Física de Superficies e Interfaces, Universidad Nacional del Litoral and CONICET, Santa Fe, Argentina
[b] Departamento de Materiales, Facultad de Ingeniería Química, Universidad Nacional del Litoral, Santa Fe, Argentina
[c] INFIQC, Universidad Nacional de Córdoba and CONICET, Departamento de Fisicoquímica, Facultad de Ciencias Químicas, Córdoba, Argentina

ARTICLE INFO

Keywords:
Hyperbranched polymer
Impedimetric determination
Thermal transition
Confined molecules
Hydrogen-bond

ABSTRACT

The thermal transitions of confined polymers are important for their applications in nanoscale devices and innovative technologies. However, thermal transitions of ultra-thin polymer assemblies confined in sub-nanometer spaces are unwell understood. In this work, the self-assembly of hyperbranched polyester-polyol polymers (HPP) immobilized on carbon surfaces were investigated. The physicochemical properties and thermal transitions of the polymers under confinement were revealed by cyclic voltammetry, electrochemical impedance spectroscopy and atomic force microscopy. The adsorption of HPP with hydroxyl-terminal groups on the bare carbon surface followed typical porous solid isotherm due to hydrogen-bond forces. The dependence of the HPP nanometer-sized layers against temperature revealed a phase transition at *ca.* 306 K. This phase transition can be explained in terms of polymer layer reorganization due to the temperature effect on the intermolecular hydrogen-bonding instead of a glass transition. This feature is of particular relevance for further applications of hyperbranched polymers thin films in nanodevices.

1. Introduction

In recent years, highly branched dendritic polymers have gained more consideration due to their exceptional properties, which differ significantly from their linear counter parts, e.g. multiple terminal functional groups, specific rheological properties based on their globular structure, and well-defined internal cavities available to encapsulate guest molecules. In particular, the facile synthesis of hyperbranched polymers has opened a door to the design of a large variety of new dendritic molecules [1] that promise to be strong competitors against other dendritic polymers like dendrimers in numerous applications, e.g. antifouling coatings [2], chemical sensing [3,4], rheological additives [5–7], drug carriers [8–11], theranostic devices [12,13], enhanced oil recovery [14], corrosion inhibition [15], micro and nanoscale patterning [16], cellular engineering [17], solar cell [18], energy storage [19], among others. In many of these applications, hyperbranched polymers are supported as thin films on different substrates or as a part of nanocomposites, and thus, could exhibit different properties from those of the bulk. For example, Bansal *et al.* showed that thermomechanical responses of polymers, which provide limitations to their practical use, are favourably altered by the addition of trace amounts of a nanofiller in nanocomposites, and they proposed that glass-transition processes in confined geometries require the interaction of near-surface regions of altered mobility.[20] According to Russell et al. [21] the film thickness introduces confinement effects on the morphology which can result on changes in the fundamental lengths scale of the morphology or even changes in the phase behaviour of polymers [22]; as the degrees of confinement increase, totally new morphologies could emerge along with changes in the chain dynamics [23].

The thermal properties of polymeric materials are important for the proper function of components and as far as we know, thermal transitions of ultra-thin hyperbranched polymer layers confined in nanometer spaces are still rather unknown. Recent studies have shown that glass transition temperature of polymers (Tg) can also be modified by tuning the attractive interactions between the polymer and the substrate involved in thin films [24] and/or nanocomposites studies [25]. In this paper, a versatile family of hyperbranched polyester-polyols polymers is employed to analyze their thermal properties when they are assembled as thin films on carbon surfaces. The physicochemical properties and thermal transitions of the polymers under confinement are revealed by cyclic voltammetry (CV), electrochemical impedance spectroscopy (EIS) and atomic force microscopy (AFM).

* Corresponding author.
E-mail address: verobrunetti@unc.edu.ar (V. Brunetti).

https://doi.org/10.1016/j.eurpolymj.2018.03.021
Received 29 November 2017; Received in revised form 12 March 2018; Accepted 13 March 2018
Available online 14 March 2018

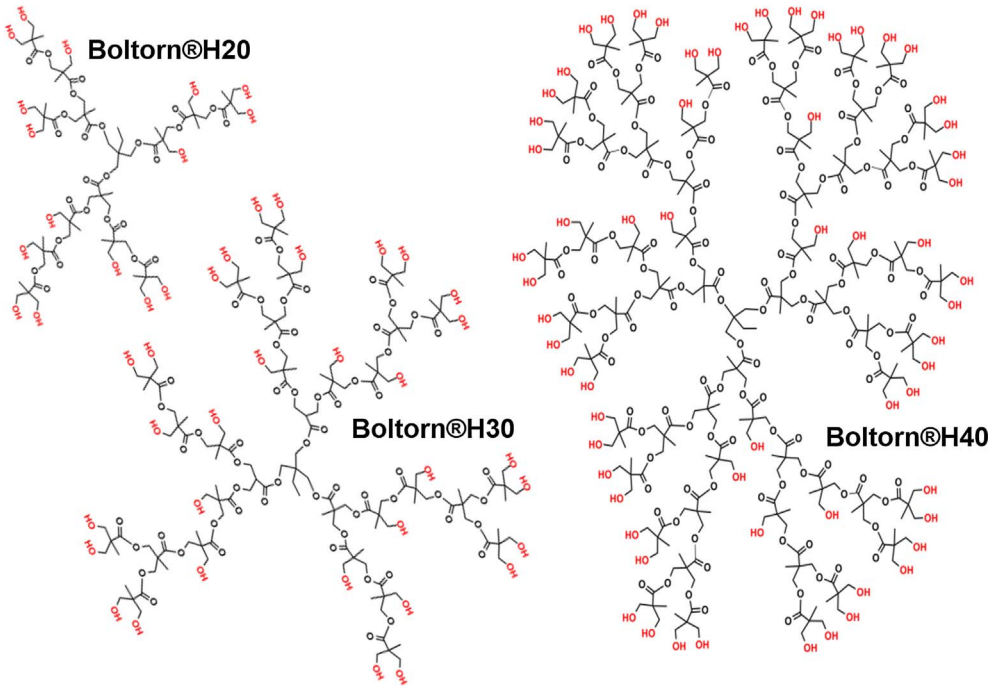

Scheme 1. Schematic representation of the hyperbranched polymers, of generation 2, 3 and 4, employed in this work.

2. Experimental section

2.1. Materials

Boltorn®H20, Boltorn®H30, and Boltorn®H40 (see scheme 1) are produced by Polymer Factory with a theoretical molecular weight of 1749.8, 3607.6, and 7323.3 g mol^{-1}, respectively. Hyperbranched polymers were prepared in dimethylsulfoxide (DMSO) solutions. Aqueous solutions of 0.1 M K_2HPO_4/KH_2PO_4 (pH 7) and 0.002 M $K_3Fe(CN)_6/K_4Fe(CN)_6$ were prepared using ultra-purified water Milli-Q equipment (Millipore). All the reagents are of analytical grade and were used without extra purification.

A 3.0 mm diameter glassy carbon electrode (GCE) purchased in CH Instruments, Inc. (Austin, TX) was employed as the working electrode for electrochemical measurements. Prior to the modification, GCE were polished using 1.0, 0.3, and 0.05 μm alumina (Buehler) and rinsed with copious Milli-Q water (Millipore Corp., USA). After polishing, the electrode was immersed in water into the ultrasonic cleaner, washed for 1 min, and subsequently dried under nitrogen flow. For microscopy studies, highly oriented pyrolytic graphite (HOPG) purchased from SPI Supplies (1 cm^2 of area and 1 mm of thickness) are used as substrates due to the average roughness of polished GCE is too high (about 20 nm) to evaluate the molecular adsorption. The HOPG substrates prior to the modification were exfoliated using adhesive tape, 3M®.

The carbon surfaces were modified by simple incubation of the substrate (GCE or HOPG) in DMSO solutions containing the hyperbranched polymer and subsequently washed with ethanol and water. This process was performed varying the conditions of incubation (polymer concentration-up to 80 mM- or time), the surfaces were rinsed promptly and immediately employed in the measurements.

2.2. Instrumentation

The electrochemical experiments were carried out in a conventional cell of three electrodes containing the working electrode (GCE), a platinum wire for the counter electrode and Ag/AgCl/Cl^- (3M) as the reference electrode. The electrolytes were deaerated under Nitrogen flux for 10 min previous to their use. A multifunctional electrochemical analyzer (CH Instruments Inc.) was employed to carry out the electrochemical measurements. Cyclic voltammograms were measured in the range of 0 to 0.60 V with a scan rate of 0.10 V s^{-1}. The impedance spectra were obtained at the open circuit potential with an amplitude of 10 mV in the frequency range from 100 KHz up to 0.1 Hz. Zview® software from Scribner Associates Inc. was employed to analyze the impedance data.

A commercial Nanotec Electronic SPM System with a PLL/dynamic measurement board operating in tapping mode was employed to acquire AFM images at room temperature and atmosphere conditions. Rotated monolithic All-In-One-Al Budget Sensors cantilevers (Innovative Solutions Bulgaria Ltd., Bulgaria) made of silicon with a 30 nm thick aluminium reflex coating. Cantilevers with resonant frequencies of 80 ± 30 and 150 ± 80 kHz, nominal spring constant in the ranges of 0.4–10 and 1–29 N/m respectively, and a radius of curvature minor than 10 nm (as informed by the commercial supplier), were used independently. The acquisition and processing of images with a resolution of 512 point/line were done using the free software WS × M 5.0® [26]. The data for roughness, skewness and kurtosis are taken from 3 or 4 specific areas in each image in order to avoid the effect of HOPG step-edges in the analysis.

3. Results and discussion

3.1. Spontaneously self-assembly of Boltorn®H30 on carbon surfaces

These molecules have a roughly globular form in solution with an average diameter of about 3 nm [27]. The incubation of carbon substrates in Boltorn®H30 solutions for only a few seconds and subsequently rinsed, results in spontaneously nanometer-scale HPP patches as those showed in Fig. 1(a) and (b). These layers in the early incubation stages grow following a sort of fractal-like structure, initially with heights of approximately of 0.8 and 1.6 nm, respectively, as it is observed in the cross-section profiles of Fig. 1(e) and (f). When the incubation time is increased up to 15 min, it evolves to a densely packed worm-like bilayer structure with a thickness of about 1.6 nm, as it is observed in Fig. 1(c), and the corresponding cross-section profile (Fig. 1(g)). It is important to notice that, even at longer incubation

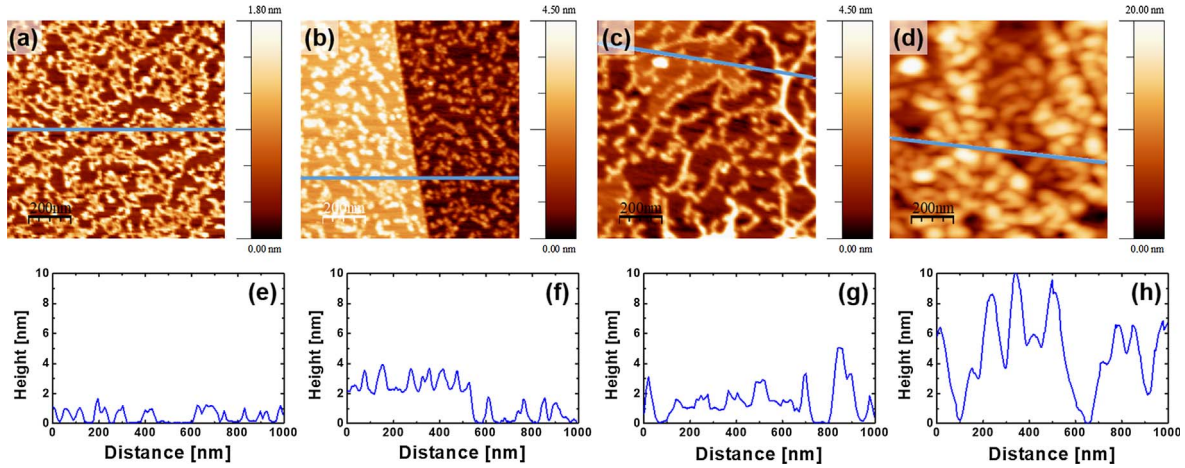

Fig. 1. Topographical AFM images (1000 nm × 1000 nm) of HOPG incubated in 0.025 M Boltorn®H30/DMSO solutions for (a) 0.5, (b) 1.5, (c) 15.0 and (d) 270.0 min. The cross sections obtained along the lines in (a–d) are depicted in graphs (e–h), respectively.

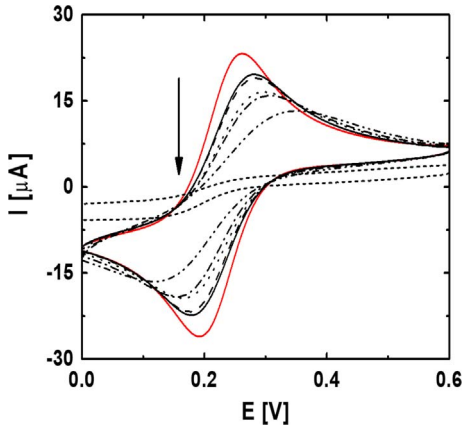

Fig. 2. Cyclic voltammograms for a GCE (solid line) and Boltorn®H30/GCE (dashed line) in 0.1 M PBS (pH 7) containing 2 mM $K_3Fe(CN)_6$ at 0.1 V s^{-1} at increasing incubation times (pointed by the arrow): 1, 5, 15, 24, 60 and 1440 min.

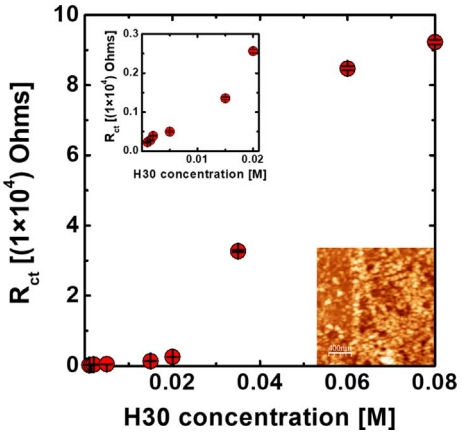

Fig. 4. R_{ct} estimated from Nyquist plots of Boltorn®H30/GCEin 0.1 M PBS (pH 7) containing 2 mM $K_3Fe(CN)_6$ at different concentrations of the Boltorn®H30/DMSO solution. Inset: enlarged graphic of the first region of the plot, and a topographical AFM image (2000 nm × 2000 nm) (full Z scale 25.0 nm) acquired at the conditions pointed out by the arrow.

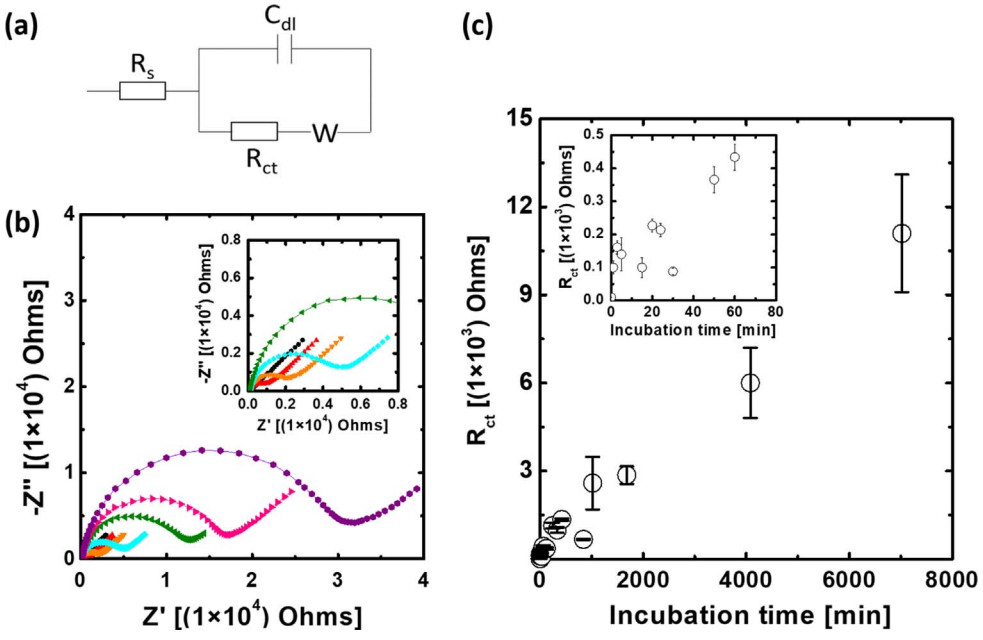

Fig. 3. (a) Scheme of the Randles equivalent circuit, (b) Nyquist plots for GCE (●) and Boltorn®H30/GCE (▲) in 0.1 M PBS (pH 7) containing 2 mM $K_3Fe(CN)_6$ at different incubation times: 2, 4, 17, 18, 28 and 68 h (1, 5, 20, 30, 50, 60 min in the insets); (c) R_{ct} calculated from non-linear least square fits of the Nyquist plots employing the Randles equivalent circuit. Insets show enlarged graphics of the first region of each plot.

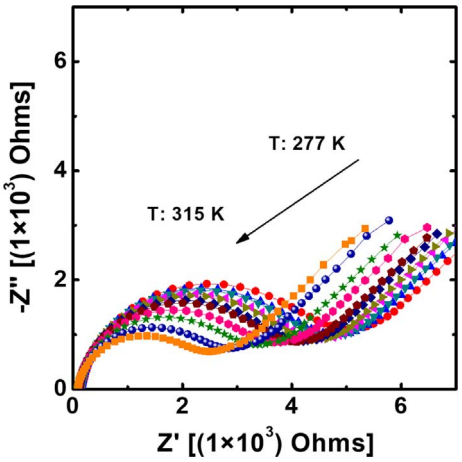

Fig. 5. Dependence against temperature of Nyquist plots for GCE (●) and Boltorn®H30/GCE (▲) in 0.1 M PBS (pH 7) containing 2 mM $K_3Fe(CN)_6$.

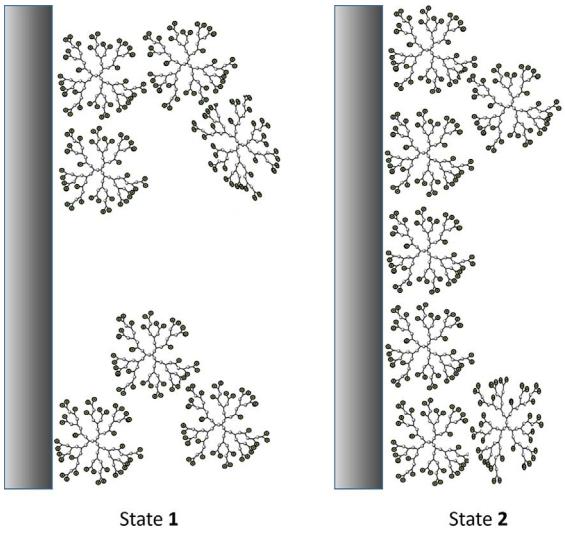

Scheme 2. Idealized scheme of hyperbranched molecules at different temperatures: state **1** at room temperature and state **2** at temperature above T_{tr}.

times, there are regions where the substrate is naked. After more than four hours of incubation, although this is not so evident in Fig. 1(d), the cross-section profile (Fig. 1(h)) reveals a surface with structures more than three or four layers high, even before a complete coalescence of the first monolayer occurs, evidencing stronger adsorbate-adsorbate instead of adsorbate-substrate interactions, probably due to hydrogen-bond forces between the hydroxyl groups and ester oxygens with neighbour hyperbranched molecules.

The adsorption kinetics of Boltorn®H30 was followed by electrochemical techniques, taking into account or following the effect of the HPP layer on the charge transfer of a redox-active probe. Fig. 2, shows the cyclic voltammetry profiles of modified glassy carbon electrodes in $Fe(CN)_6^{3-}/Fe(CN)_6^{4-}$ solutions varying the incubation time. The presence of the HPP layer partially inhibits the charge transfer of the redox probe at lower incubation times, evidenced by a shift of the anodic and cathodic peaks to more positive and negative potential correspondingly, and a decrease of the coulometric charge up to a totally blocked behaviour observed at incubation times of about 24 h.

EIS has been widely used to study the interfacial and transport properties of films and offers the opportunity to monitor the adsorption kinetics of the HPP with an enhanced sensibility regarding CV, with the aid of a redox-active label such as ferro/ferricyanide one. Fig. 3 shows typical electrochemical impedance spectra of modified electrodes varying the incubation time. The Nyquist plots show semicircles in the high frequency region and, a roughly 45° straight line in the low frequency one. The results were analyzed by applying non-linear least square fits with a Randles equivalent electrical circuit (see scheme in Fig. 3) including the solution resistance (R_s), the charge transfer resistance of the film (R_{ct}), the double layer capacitance (C_{dl}) and Warburg impedance (W) associated with a semi-infinite linear diffusion [28]. The charge transport mechanism might involve either movement of the electroactive ions by diffusion or hopping/tunnelling of electrons from one redox-site to a next one at fixed positions in the polymer chain [29]. In Fig. 3 (b), the dependence of R_{ct} as a function of incubation time exhibits a continuous increase without reaching a plateau, in good accordance with the presence of multilayers.

Table 1
Thermal properties of Boltorn® polymers.

HPP	T_{tr} [K]	E_a, State 1 [kJ/mol]	E_a, State 2 [kJ/mol]	T_g [K][a]
Boltorn®H20	307	11.0	26.5	287
Boltorn®H30	306	9.7	44.4	308
Boltorn®H40	307	10.1	37.1	319

[a] T_g values of HPP in bulk obtained by DSC and reported by Androulaki et al. [31].

Fig. 4 shows the plot of R_{ct} against concentration after incubation of the electrodes in Boltorn®H30/DMSO solutions for long times. The dependence of R_{ct} on the HPP concentration, clearly exhibits an isotherm typically associated to the adsorption of porous solids [30], in good agreement with the AFM image which exhibits an incomplete multilayers growth of HPP onto the carbon substrate after more than 4 h of incubation.

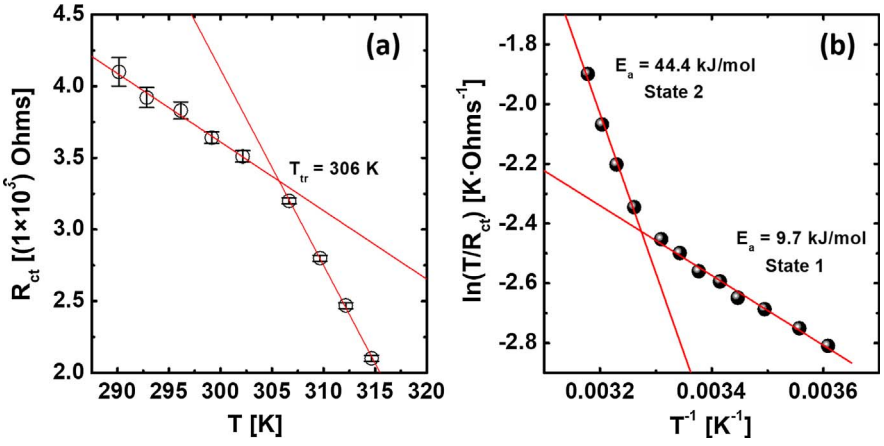

Fig. 6. (a) R_{ct} as a function of temperature for Boltorn®H30 thin films on GCE. R_{ct} was obtained from non-linear least square fits of Nyquist plots shown in Fig. 5 employing the Randles equivalent circuit. (b) Arrhenius-type plot showing the dependence of $\ln(T/R_{ct})$ as a function of the inverse of temperature (T^{-1}). At $T = T_{tr}$, a noticeable difference in the slope of the correlation line is observed, indicative of a higher activation energy, Ea.

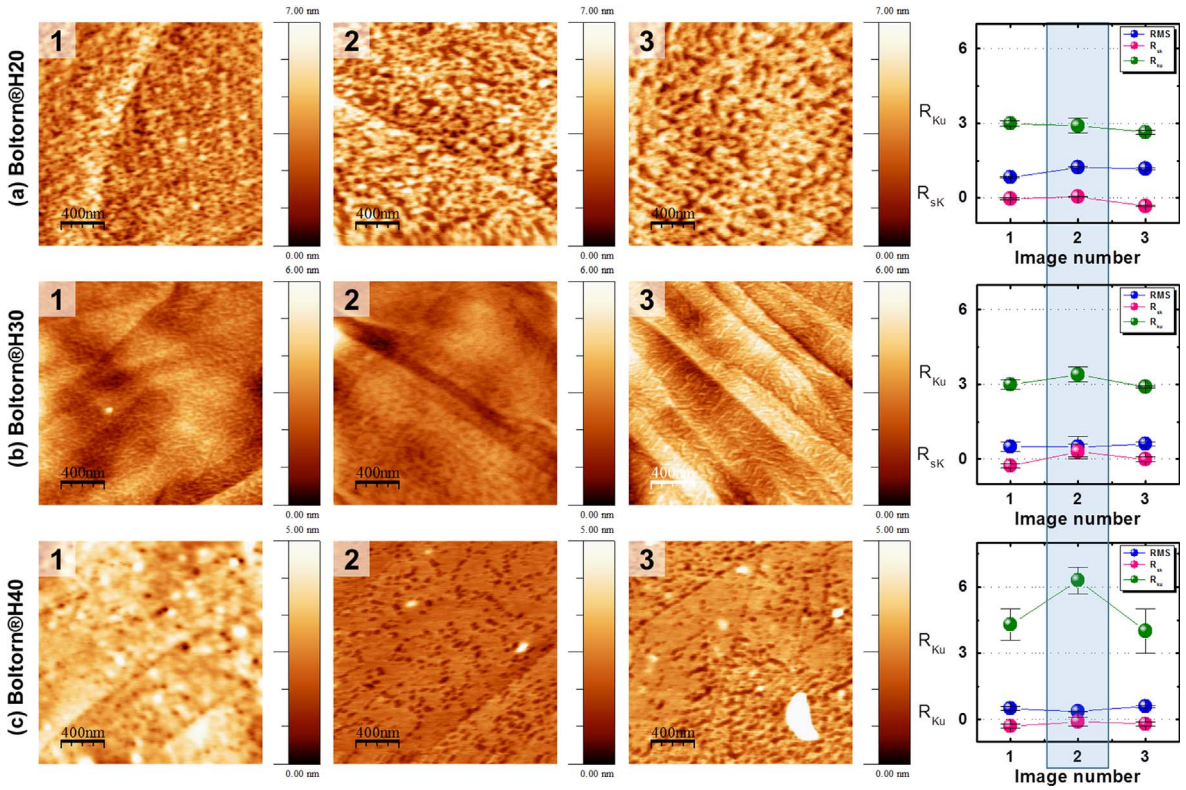

Fig. 7. Topographical AFM images (2000 nm × 2000 nm) of HOPG modified by. ((a) Boltorn®H20 (Generation 2), (b) Boltorn®H30 (Generation 3), and (c) Boltorn®H40 (Generation 4) at State **1** (room temperature), State **2** (immediately after heating up to 318 K), and State **3** (after cooling down to room temperature), respectively. The plots on the right illustrate the statistical parameters calculated from AFM images acquired at each state.

3.2. Thermal properties of the HPP layers

Fig. 5 shows the dependence of Nyquist plots as a function of temperature for GCE modified with Boltorn®H30. It is clearly observed that semicircles associated with the R_{ct} values decrease rapidly upon heating above room temperature. The reorganization and higher mobility of polymer chains promotes the movement of redox probes closely to the proximity of the electrode surface and also the charge propagation across the film.

The transition temperature called T_{tr} was obtained from the intersection of two lines extrapolated from low and high temperature regions on the R_{ct} against temperature plot, shown in Fig. 6(a). For Boltorn®H30 films a T_{tr} value of 306 K is obtained, which is similar to the reported glass transition temperature (T_g = 308 K) of Boltorn®H30 measured by differential scanning calorimetry [31]. However, the phase transition in this case is completely different, as it will be described below. Fig. 6(b) shows the Arrhenius-type plot based on the data reported in Fig. 6(a), in which the dependence of $\ln(T/R_{ct})$ as a function of the inverse of the temperature (T^{-1}) is shown. Differences between both thermal regimes, State **1** (low T regime) and State **2** (high T regime), are clearly manifested by a well-defined variation in the activation energy for the electron transfer process of the redox probe. From the slopes in Fig. 6(b), activation energies of $E_{a,State1}$ = 9.7 kJ/mol and $E_{a,State2}$ = 44.4 kJ/mol were calculated for State **1** and State **2**, respectively. These values clearly prove that phase transition from State **1** to State **2** is not a "glassy" to "rubbery" state transition, in spite of the similar values obtained for T_{tr} compared to the reported T_g one for Boltorn®H30 in bulk, showing that significant differences emerge when molecules are confined to distances comparable to their sizes. At higher temperatures, the impact of connectivity, structure, and chain environment on molecular motion at the length scale of a few monomers is constrained by higher polymer-substrate interactions and thus, state 2 presents a higher activation energy than state 1. The phase transition from State **1** to State **2** could be explained as a reorganization of the HPP molecules from a porous multilayer to a more compact layer, probably due to a weakening of the existing H-bond network and, consequently, followed a major mobility of the polymer molecules due to heating, favouring the interaction between adsorbates and substrate (see Scheme 2). Moreover, in contrast to T_g values reported for HPP in bulk, no significant differences are observed for T_{tr} values for different generation HPP immobilized on GCE, as it can be observed in Table 1 (see supporting information). Also, it is seen that while $E_{a,State1}$ value is fairly constant, $E_{a,State2}$ value changes for all HPP generations. The formation of a more compact HPP layer makes evident a dependency with the HPP generation, probably due to the formed new H-bonds at State **2**. The increment of the $E_{a,State2}$ from the second to the third generation could be associated with an increase in the intermolecular H-bond, while the decrease of $E_{a,State2}$ for the fourth generation might be related with a major number of intramolecular H-Bond interactions. Androulaki et al. [31] reported a significant dependence of T_g values of pure HPP depending on its generation, as a consequence of the molecular weight increase and higher degree of branching, and significant alterations in their behaviour under confinement in nanocomposites, where HPP are intercalated within the galleries of natural montmorillonite. Heating hyperbranched polyesters above T_g leads to a weakening of non-covalent interactions and, consequently, to a major mobility of molecules.

In order to gain insight into thermal properties of HPP layers, the reorganization of the porous layer after heating was investigated by AFM. Fig. 7 shows the topographical AFM images of modified carbon surfaces in three states: room temperature (State **1**), immediately after heating up to 318 K (State **2**), and after cooling down to room temperature again (State **3**). Statistical parameters calculated from AFM images are depicted also in Fig. 7. The root mean square roughness (RMS) values are not too sensitive, but also denote changes around T_{tr} showing a slight decrease at temperatures above T_{tr} for HPP of

generations 3 and 4, and a minor increment for generation 2. Surface skewness (R_{sk}) is a measure of the statistical distribution symmetry of a surface profile. A symmetric distribution should have skewness values near zero, which means that it has evenly distributed peaks and valleys in height [32]. Thus, the R_{sk} parameter gives an indication of the existence of deep valleys and/or sharp peaks. While surfaces with larger valleys than peaks present negative skewness values, quite the opposite, surfaces with higher peaks than valleys would be characterized by positive skewness values. From Fig. 7(a)–(c), it should be noticed that R_{sk} values are around zero at room temperature for generation 2, while for generations 3 and 4 is slightly negative. R_{sk} increase for generations 3 and 4, even becoming positive for generation 3 at temperatures above T_{tr}. On the contrary, for generation 2 it has an almost indiscernible increase. Upon retracing at room temperature, negative skewness values were found in all cases. Surface kurtosis (R_{ku}) is a measure of the "spikiness" of the surface, or the distribution of spikes above and below the mean line; it is also a measure of the randomness of surface heights and takes a value of 3 for the normal distribution. For $R_{ku} < 3$ the surface is dominated by sharp peaks, whereas if $R_{ku} < 3$ the peaks are bumpy [33]. In good agreement with EIS data, the topographical AFM images at temperatures above the T_{tr} exhibit an increase in the R_{ku} values, denoting a reorganization of the HPP layer after the rupture of hydrogen-bonding between adsorbates. This change is greater for generation 4 than for generation 3, but always is reversible. The R_{ku} value of generation 2 only exhibited a greater dispersion at high temperature, followed by a decrease to a value below 3 after retrace at room temperature, indicating a bumpy surface.

4. Conclusions

The self-assembly of hyperbranched polyester-polyol polymers immobilized on carbon surfaces were investigated by cyclic voltammetry, electrochemical impedance spectroscopy and atomic force microscopy, focusing on thermal transitions of the polymers under confinement. The adsorption of hyperbranched polymers with hydroxyl-terminal groups on the bare carbon surface followed a typical behaviour of an isotherm corresponding to a porous solid. The polymers form incomplete multilayers probably due to hydrogen-bond forces between adsorbates. The evolution of the nanometer-sized layers with temperature revealed a phase transition at *ca.* 306 K, for HPP of generations 2, 3 and 4. The phase transition can be explained as a film reorganization due to temperature effects on hydrogen-bonding. This feature is of particular relevance for further application of hyperbranched polyol-polymers as thin films or coatings.

Acknowledgements

We wish to express our gratitude to the Physics of Surfaces and Interfaces Laboratory (IFIS Litoral, UNL-CONICET, Santa Fe, Argentina) for the use of their SPM equipment. Financial support from CONICET (PIP 2012-2014 N°577), ANPCyT (PICT 2015-2477), and SECYT-UNC are gratefully acknowledged. E.D.F. thanks CONICET for the fellowship.

Appendix A. Supplementary material

Supplementary data associated with this article can be found, in the online version, at https://doi.org/10.1016/j.eurpolymj.2018.03.021.

References

[1] P. Viville, A. Deffieux, M. Schappacher, J.L. Bredas, Surface organization of single hyperbranched polymer molecules, as studied by atomic force microscopy, Mater. Sci. Eng. C 15 (2001) 311–314.
[2] Y. Yu, H. Frey, Controllable nonspecific protein adsorption by charged hyperbranched polyglycerol thin films, Langmuir 31 (2015) 13101–13106, http://dx.doi.org/10.1021/acs.langmuir.5b03243.
[3] C.P. Sen, V. Devendar Goud, R.G. Shrestha, L.K. Shrestha, K. Ariga, S. Valiyaveettil, BODIPY based hyperbranched conjugated polymers for detecting organic vapors, Polym. Chem. 7 (2016) 4213–4225, http://dx.doi.org/10.1039/C6PY00847J.
[4] X. Ma, F. Tao, Y. Zhang, T. Li, F.M. Raymo, Y. Cui, Detection of nitroaromatic explosives by a 3D hyperbranched σ–π conjugated polymer based on a POSS scaffold, J. Mater. Chem. A 5 (2017) 14343–14354.
[5] X. Fei, W. Wei, Y. Tang, Y. Zhu, J. Luo, M. Chen, X. Liu, Simultaneous enhancements in toughness, tensile strength, and thermal properties of epoxy-anhydride thermosets with a carboxyl-terminated hyperbranched polyester, Eur. Polym. J. 90 (2017) 431–441, http://dx.doi.org/10.1016/j.eurpolymj.2017.03.022.
[6] J.W. Robinson, Y. Zhou, P. Bhattacharya, R. Erck, J. Qu, J.T. Bays, L. Cosimbescu, Probing the molecular design of hyper-branched aryl polyesters towards lubricant applications, Sci. Rep. 6 (2016) 18624, http://dx.doi.org/10.1038/srep18624.
[7] M.M. Eissa, M.S.A. Youssef, A.M. Ramadan, A. Amin, Poly(ester-amine) hyperbranched polymer as toughening and co-curing agent for epoxy/clay nanocomposites, Polym. Eng. Sci. 53 (2013) 1011–1020, http://dx.doi.org/10.1002/pen.
[8] R. Albrecht, S. Fehse, K. Pant, S. Nowag, H. Stephan, R. Haag, C.C. Tzschucke, Polyglycerol-based copper chelators for the transport and release of copper ions in biological environments, Macromol. Biosci. 16 (2016) 412–419, http://dx.doi.org/10.1002/mabi.201500284.
[9] Y. Yang, K. Achazi, Y. Jia, Q. Wei, R. Haag, J. Li, Complex assembly of polymer conjugated mesoporous silica nanoparticles for intracellular pH-responsive drug delivery, Langmuir 32 (2016) 12453–12460, http://dx.doi.org/10.1021/acs.langmuir.6b01845.
[10] E. Yildirim, Y. Zhang, J.L. Lutkenhaus, M. Sammalkorpi, Thermal transitions in polyelectrolyte assemblies occur via a dehydration mechanism, ACS Macro Lett. 4 (2015) 1017–1021, http://dx.doi.org/10.1021/acsmacrolett.5b00351.
[11] L. Zhang, Y. Zhou, G. Shi, X. Sang, C. Ni, Preparations of hyperbranched polymer nano micelles and the pH/redox controlled drug release behaviors, Mater. Sci. Eng. C 79 (2017) 116–122, http://dx.doi.org/10.1016/j.msec.2017.05.027.
[12] A. Mashhadi Malekzadeh, A. Ramazani, S.J. Tabatabaei Rezaei, H. Niknejad, Design and construction of multifunctional hyperbranched polymers coated magnetite nanoparticles for both targeting magnetic resonance imaging and cancer therapy, J. Colloid Interface Sci. 490 (2017) 64–73, http://dx.doi.org/10.1016/j.jcis.2016.11.014.
[13] P. Sun, D. Chen, H. Deng, N. Wang, P. Huang, X. Jin, X. Zhu, "Bottom-up" construction of multi-polyprodrug-arm hyperbranched amphiphiles for cancer therapy, Bioconjug. Chem. 28 (2017) 1470–1480, http://dx.doi.org/10.1021/acs.bioconjchem.7b00146.
[14] W.F. Pu, R. Liu, K.Y. Wang, K.X. Li, Z.P. Yan, B. Li, L. Zhao, Water-soluble core-shell hyperbranched polymers for enhanced oil recovery, Ind. Eng. Chem. Res. 54 (2015) 798–807, http://dx.doi.org/10.1021/ie5039693.
[15] E. Armelin, R. Whelan, M.Y. Martinez-Triana, C. Aleman, M.G. Finn, D. Diaz, Protective coatings for aluminum alloy based on hyperbranched 1,4-polytriazoles, ACS Appl. Mater. Interfaces 9 (2017) 4231–4243, http://dx.doi.org/10.1021/acsami.6b14174.
[16] E. Moore, B. Delalat, R. Vasani, H. Thissen, N.H. Voelcker, Patterning and biofunctionalization of antifouling hyperbranched polyglycerol coatings, Biomacromolecules 15 (2014) 2735–2743, http://dx.doi.org/10.1021/bm500601z.
[17] S. Wang, R. Chen, PH-responsive, lysine-based, hyperbranched polymers mimicking endosomolytic cell-penetrating peptides for efficient intracellular delivery, Chem. Mater. 29 (2017) 5806–5815, http://dx.doi.org/10.1021/acs.chemmater.7b00054.
[18] J. Zhang, S. Xie, X. Zhang, Z. Lu, H. Xiao, C. Li, G. Li, X. Xu, X. Chen, Z. Bo, Hyperbranched polymer as an acceptor for polymer solar cells, Chem. Commun. 53 (2017) 537–540, http://dx.doi.org/10.1039/C6CC07335B.
[19] B.J. Yik, M. Guo, Y. Kwon, T. Goodson, New approaches for energy storage with hyperbranched polymers, J. Phys. Chem. C 121 (2017) 7108–7122, http://dx.doi.org/10.1021/acs.jpcc.7b00781.
[20] A. Bansal, H. Yang, C. Li, K. Cho, B.C. Benicewicz, S.K. Kumar, L.S. Schadler, Quantitative equivalence between polymer nanocomposites and thin polymer films, Nat. Mater. 4 (2005) 693–698, http://dx.doi.org/10.1038/nmat1447.
[21] T.P. Russell, Y. Chai, 50th Anniversary perspective: putting the squeeze on polymers: a perspective on polymer thin films and interfaces, Macromolecules 50 (2017) 4597–4609, http://dx.doi.org/10.1021/acs.macromol.7b00418.
[22] D. Cangialosi, A. Alegría, J. Colmenero, Effect of nanostructure on the thermal glass transition and physical aging in polymer materials, Prog. Polym. Sci. 55 (2016) 128–147.
[23] S. Napolitano, E. Glynos, N.B. Tito, Glass transition of polymers in bulk, confined geometries, and near interfaces, Reports Prog. Phys. 80 (2017) 36602, http://dx.doi.org/10.1088/1361-6633/aa5284.
[24] S.S. Kharintsev, E.A. Chernykh, A.I. Fishman, S.K. Saikin, A.M. Alekseev, M.K. Salakhov, Photoinduced heating of freestanding azo-polymer thin films monitored by scanning thermal microscopy, J. Phys. Chem. C 121 (2017) 3007–3012, http://dx.doi.org/10.1021/acs.jpcc.6b12658.
[25] M.C. Biswas, S. Jeelani, V. Rangari, Influence of biobased silica/carbon hybrid nanoparticles on thermal and mechanical properties of biodegradable polymer films, Compos. Commun. 4 (2017) 43–53, http://dx.doi.org/10.1016/j.coco.2017.04.005.
[26] I. Horcas, R. Fernández, J.M. Gómez-Rodríguez, J. Colchero, J. Gómez-Herrero, A.M. Baro, WSXM: a software for scanning probe microscopy and a tool for nanotechnology, Rev. Sci. Instrum. 78 (2007), http://dx.doi.org/10.1063/1.2432410.
[27] E. Zagar, M. Zigon, Aliphatic hyperbranched polyesters based on 2, 2-bis (methylol) propionic acid—determination of structure, solution and bulk properties, Prog. Polym. Sci. 36 (2011) 53–88, http://dx.doi.org/10.1016/j.progpolymsci.2010.08.004.
[28] A.J. Bard, L.R. Faulkner, Electrochemical Methods Fundamentals and Applications, second ed., JOHN WILEY & SONS, INC., New York, 2001.

[29] J.M. Giussi, O. Azzaroni, S. Hensel-Bielowka, Z. Wojnarowska, J. Knapik, M. Paluch, Synthesis, characterization and dielectric relaxation study of hyperbranched polymers with different molecular architecture, Polymer (Guildf) 100 (2016) 227–237, http://dx.doi.org/10.1016/j.polymer.2016.08.027.

[30] K.S.W. Sing, Reporting physisorption data for gas/solid systems with special reference to the determination of surface area and porosity (Provisional), Pure Appl. Chem. 54 (1982), http://dx.doi.org/10.1351/pac198254112201.

[31] K. Androulaki, K. Chrissopolou, D. Prevosto, M. Labardi, S.H. Anastasiadis, Dynamics of hyperbranched polymers under confinement – a dielectric relation study, ACS Appl. Mater. Interfaces 7 (2015) 12387–12398, http://dx.doi.org/10.1021/am507571y.

[32] Y. Chen, W. Huang, Numerical simulation of the geometrical factors affecting surface roughness measurements by AFM, Meas. Sci. Technol. 15 (2004) 2005–2010, http://dx.doi.org/10.1088/0957-0233/15/10/010.

[33] M. Zecchino, Veeco Instruments Inc., Characterizing surface quality: why average roughness is not enough, Bruker Appl. Notes., 2010, pp. 1–4, < https://www.bruker.com/fileadmin/user_upload/8-PDF-Docs/SurfaceAnalysis/3D-OpticalMicroscopy/ApplicationNotes/AN511-Characterizing_Surface_Quality-Why_Average_Roughne.pdf > .